Rtt109 promotes nucleosome replacement ahead of the replication fork

Felix Jonas, Gilad Yaakov and Naama Barkai

Genome Res. 2022 32: 1089-1098 originally published online May 24, 2022
Access the most recent version at doi:10.1101/gr.276674.122

Rtt109 promotes nucleosome replacement ahead of the replication fork

Felix Jonas,[1,2] Gilad Yaakov,[1,2] and Naama Barkai[1]

[1]*Department of Molecular Genetics, Weizmann Institute of Science, Rehovot 7610001, Israel*

DNA replication perturbs chromatin by triggering the eviction, replacement, and incorporation of nucleosomes. How this dynamic is orchestrated in time and space is poorly understood. Here, we apply a genetically encoded sensor for histone exchange to follow the time-resolved histone H3 exchange profile in budding yeast cells undergoing slow synchronous replication in nucleotide-limiting conditions. We find that new histones are incorporated not only behind, but also ahead of the replication fork. We provide evidence that Rtt109, the S-phase-induced acetyltransferase, stabilizes nucleosomes behind the fork but promotes H3 replacement ahead of the fork. Increased replacement ahead of the fork is independent of the primary Rtt109 acetylation target H3K56 and rather results from Vps75-dependent Rtt109 activity toward the H3 N terminus. Our results suggest that, at least under nucleotide-limiting conditions, selective incorporation of differentially modified H3s behind and ahead of the replication fork results in opposing effects on histone exchange, likely reflecting the distinct challenges for genome stability at these different regions.

[Supplemental material is available for this article.]

Eukaryotic DNA is wrapped around histone octamers to form nucleosomes, the basic building blocks of chromatin (Luger et al. 1997). Nucleosomes limit access to the DNA, thus protecting the genome and providing a unified platform for regulating DNA-based processes (Kristjuhan and Svejstrup 2004; Schwabish and Struhl 2004; Bondarenko et al. 2006; Fleming et al. 2008; Lai and Pugh 2017). Regulatory mechanisms act on chromatin to change nucleosome positioning along the DNA and to modify histone residues for controlling the recruitment of regulatory factors or histone–DNA affinity (Bannister and Kouzarides 2011; Owen-Hughes and Gkikopoulos 2012). Acetylation of histones on their N terminus, for example, can mediate the recruitment of chromatin remodelers such as the SWI/SNF or RSC complexes to regulate access to DNA (Hong et al. 1993; Lee et al. 1993; Bauer et al. 1994; Zhang et al. 2010; Chatterjee et al. 2011). Complementing these mechanisms that act on DNA-bound histones is the process of nucleosome exchange in which histone chaperones and remodelers evict or replace DNA-bound histones (Laskey et al. 1978; Dilworth and Dingwall 1988; Ito et al. 1996; Verreault et al. 1996; Andrews and Luger 2011; Hsieh et al. 2013; Mattiroli et al. 2015; Clapier et al. 2017; Hammond et al. 2017). Histone exchange reshapes the epigenetic landscape by diluting position-dependent marks while enriching for modifications present in the unbound histone pool.

Nucleosome dynamics are particularly prominent during DNA replication (Groth et al. 2007; Hamperl and Cimprich 2016). In addition to the increase of nucleosomes needed for wrapping newly synthesized DNA, progression of the replication fork requires nucleosomes to disassemble, at least transiently. Nucleosome disassembly is required at actively replicating locations, but nucleosome replacement could also extend to regions ahead of the fork, where accumulated helical tensions may evict nucleosomes (as shown during transcription) (Corless and Gilbert 2016), exposing DNA to potential damage. Finally, enzymes expressed in S phase modify histones before DNA incorporation, and these specifically modified histones become enriched on newly synthesized DNA, shaping an epigenetic landscape unique to replication with possible consequences on chromatin dynamics.

The acetyltransferase Rtt109 is a central regulator of the replication-specific epigenetic landscape in budding yeast. It is the sole acetyltransferase that acetylates newly synthesized histones on their internal H3K56 residue and also acetylates multiple N-terminal H3 residues (Han et al. 2007; Tsubota et al. 2007; Berndsen et al. 2008; Fillingham et al. 2008). The histone chaperone Asf1 is required for both H3K56 and H3 N-terminal acetylation by Rtt109, whereas another chaperone, Vps75, is required only for the latter (Berndsen et al. 2008; Fillingham et al. 2008). Of note, although both modifications are added before incorporation onto DNA, their genomic profile and temporal stability vary: H3K56 acetylation remains associated with replicated DNA until the end of S phase, when its specific deacetylase Hst3 is induced (Celic et al. 2006; Maas et al. 2006; Bar-Ziv et al. 2016; Voichek et al. 2016b, 2018). In contrast, replication-dependent acetylation of H3K9, and likely other N-terminal residues, appears as a transient wave that closely associates with, and in fact precedes, the replication fork (Bar-Ziv et al. 2016).

Functionally, cells are viable without Rtt109 but suffer from genomic instability (Driscoll et al. 2007; Li et al. 2008). The contribution of Rtt109 to additional cellular processes depends on its specific activity: H3K56 (but not H3K9) acetylation is required for expression homeostasis, namely, the transcriptional buffering of the gene dosage increase in replicated regions (compared with those not yet replicated) (Bar-Ziv et al. 2016, 2020; Voichek et al. 2016a,b, 2018). In contrast, Rtt109-dependent H3 N-terminal acetylation slows down the replication fork, a phenotype not seen in H3K56 mutants (Frenkel et al. 2021).

[2]**These authors contributed equally to this work.**
Corresponding authors: gilad.yaakov@weizmann.ac.il, naama.barkai@weizmann.ac.il
Article published online before print. Article, supplemental material, and publication date are at https://www.genome.org/cgi/doi/10.1101/gr.276674.122.

The fact that Rtt109 acts on unbound H3 suggests that it plays a role in H3 incorporation. Consistent with such a role, H3K56 acetylation increases the affinity of H3 toward CAF1, the histone chaperone incorporating histones at the replication fork (Li et al. 2008; Han et al. 2013). Genome-wide mapping of H3 exchange rates further revealed a tight correlation between histone exchange and H3K56 acetylation (Rufiange et al. 2007; Kaplan et al. 2008), and functional analysis of H3K56 mutants indicated a contribution of this modification to histone dissociation rates at particular locations (Ferrari and Strubin 2015) or in vitro (Lee and Lee 2019). However, these studies correlating H3K56ac with histone exchange at the genomic level considered nonreplicating cells, in which Rtt109 levels are lower than during replication, and H3K56ac levels are correspondingly low (Rufiange et al. 2007; Kaplan et al. 2008). As for replication-associated H3K9ac, its localization ahead of the progressing fork (Bar-Ziv et al. 2016) may suggest a contribution to H3 incorporation there (Frenkel et al. 2021), but no functional data supporting this notion are available to date.

Clarifying the role of histone exchange in expression homeostasis and replication fork slowdown requires measuring the nucleosome exchange pattern in replicating cells. Traditional techniques to assay exchange apply pulse-chase histone labeling followed by the collection of multiple time-resolved samples. These therefore involve temporal perturbations and are subject to significant time delays from histone labeling to exchange measurements, limiting their use during rapid dynamic processes such as DNA replication (Ahmad and Henikoff 2002; Keppler et al. 2004; Schermer et al. 2005; Dion et al. 2007; Rufiange et al. 2007; Kaplan et al. 2008; Verzijlbergen et al. 2010, 2011; Radman-Livaja et al. 2011; Smolle et al. 2012; Venkatesh et al. 2012; Das and Tyler 2013; Huang et al. 2013; Kraushaar et al. 2013; Ha et al. 2014; Yildirim et al. 2014; Sadeghi et al. 2015; Siwek et al. 2018). Recently, we developed a new histone exchange sensor that alleviates the need for pulse-chase by using genetically encoded exchange sensors and allows for exchange measurements during a dynamic process using a single sample (Yaakov et al. 2021). Here, we use wild-type and mutant strains carrying an H3 exchange sensor to define the time-resolved, genome-wide H3 exchange pattern during replication and further test the roles of Rtt109 and its associated H3 acetylations in regulating this exchange during replication. To increase temporal resolution, we slowed replication by subjecting cells to the nucleotide-depleting drug hydroxyurea (HU).

Results

The H3 exchange profile during replication

We engineered the H3 exchange reporter strain as previously described and validated (Yaakov et al. 2021) by fusing both H3 alleles, *HHT1* and *HHT2*, to a TEV-cleavable tag and the H2B subunit *HTB2* to the TEV protease (Methods). The H3 tags are composed of two epitopes (HA and myc) connected via a linker with a TEV cleavage site. Because H3 and H2B bind exclusively in the context of the histone octamer, myc cleavage only occurs after nucleosome formation on DNA. Accordingly, at any given genomic locus, HA levels report on nucleosome (H3) occupancy, and myc levels report on the associated H3 incorporation rate and their ratio on the exchange rate (Yaakov et al. 2021).

To enable sufficient temporal resolution, we slowed replication by subjecting cells to the deoxynucleotide-depleting drug HU. Cells carrying the H3 exchange reporter were G_1-arrested, released into medium supplemented with HU, and sampled every 10–20 min up to 3 h (Fig. 1A). DNA replication progression was measured using DNA-seq, and chromatin immunoprecipitation (ChIP-seq) was used to profile the H3 exchange tags, HA and myc, genome-wide. Using the same samples, we also mapped two Rtt109-dependent modifications, H3K56 and H3K9 acetylation.

Histone exchange is composed of replication-dependent and -independent components. The former localizes to regions surrounding the fork, whereas the latter also occurs in regions not actively replicating (associated, e.g., with transcription). To distinguish these contributions, we defined the temporal progression of DNA replication using our independent measurements of DNA content. As expected, DNA content and nucleosome abundance under nucleotide-depleted conditions increased gradually, with different genomic regions replicating at different times and in tight correlation with their annotated replication time (RT) in unperturbed S phase (Fig. 1B). Using this analysis, we defined for each time point the fraction of cells in which a given region has already been replicated (replicated fraction), and the fraction of cells in which replication is active within the current time frame (replication rate; Methods).

Examining the Rtt109-dependent marks verified the expected localization of H3K56ac to replicated regions (Fig. 1B,C). The H3K9ac profile, on the other hand, is composed of transcription and replication-dependent components, with only the latter being Rtt109 dependent (Bar-Ziv et al. 2016), and therefore requires normalization by the H3K9ac profile of nonreplicating (G_1-arrested) cells (Fig. 1B). Normalized H3K9ac localized to regions that were actively replicating but, contrasting H3K56ac, did not accumulate in replicated regions (Fig. 1C,D). Examining the temporal relation of the H3K9ac profile to the replication fork verified that, similar to that of rapidly replicating cells (Bar-Ziv et al. 2016), H3K9ac precedes the progressing fork during nucleotide-limiting slowed replication as well (Fig. 1E; Supplemental Fig. S1A).

To quantify H3 exchange, we considered the myc profile reporting on the H3 incorporation rate. As expected, once replication commenced, myc began to increase around early replicating origins and then expanded and spread to later replicating regions (Fig. 1B,C). Subsequently, the myc signal decreased in replicated regions while still localizing to actively replicating ones (Fig. 1B, C). Reduction of myc in replicated regions was partial, as it remained higher than at loci not yet replicated (Supplemental Fig. S1B). Finally, a high myc signal was also found ahead of the replication fork, similar to H3K9ac (Fig. 2A; Supplemental Fig. S1A). We conclude that the myc sensor successfully captures histone incorporation during the dynamic process of replication.

Replication rate dominates the replication-dependent H3 exchange

Different processes contribute to replication-dependent histone exchange. These include the perturbation of nucleosomes ahead of the fork and the incorporation of new histones needed for wrapping the newly synthesized DNA. In addition, nucleosome dynamics may change owing to the unique epigenetic landscape generated through replication, for example, enrichment of H3K56ac. Given evidence that replication is stochastic (Bechhoefer and Rhind 2012), these three processes overlap spatially and temporally, even in our synchronized cultures. In particular, regions of increased gene dosage (replicated in some cells) are still being actively replicated in other cells.

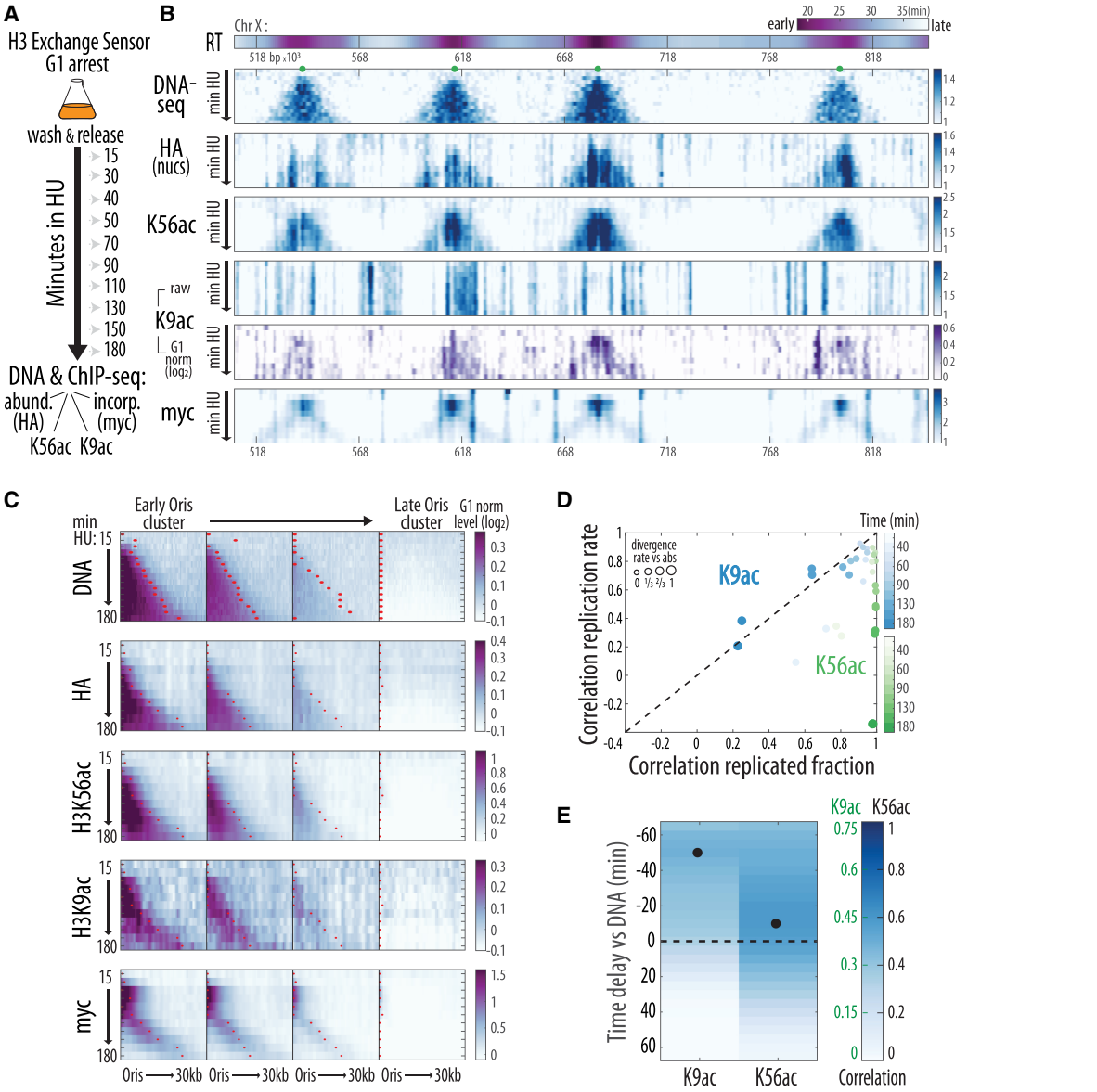

Figure 1. Chromatin replication dynamics during slowed S phase. (*A*,*B*) Profiling histone H3 modifications and exchange dynamics during slowed replication. (*A*) Time-resolved chromatin immunoprecipitation (ChIP-seq) and DNA-seq experiments were performed to follow replication in cells synchronously released into 200 mM hydroxyurea (HU) to slow replication. DNA levels, H3 abundance (HA), H3 incorporation (myc) (see Yaakov et al. 2021), and H3K56 and H3K9 acetylations were measured. (*B*) Replication dynamics are captured by the change in read coverage, shown here on a segment of Chromosome X. The annotated replication time (RT) in unperturbed S phase is included (Yabuki et al. 2002). Annotated origins of replication initiation (ORIs) (Siow et al. 2012) with RT < 21 min are shown as green dots. H3K9ac coverage is additionally shown after normalizing to that of nonreplicating, G_1-arrested cells ($\log_2$). (*C*,*D*) H3K56ac correlates with DNA abundance, whereas H3K9ac accumulates ahead of the replication fork. ORIs were clustered by their RT, and profiles around each ORI were aligned and averaged. (*C*) Shown are G_1-normalized profiles within each of the four ORI clusters (note the scales for the various antibodies) and the fork position as calculated from the DNA profile (red dots). (*D*) Data for H3K9ac or H3K56ac (n = 2 time courses) are summarized by comparing the profiles of these modifications with the DNA profile (replicated fraction) or its change along the genome (replication rate; see Methods). Color intensity indicates time, and the dot size indicates the divergence (1 − correlation) between the replicated fraction and rate. (*E*) H3K9ac accumulates ahead of the replication fork. Cross-correlation between the temporal changes of the indicated acetylation with DNA dynamics is shown as a function of the time delay; black dots indicate the delay with the highest correlation (for repeat, see Supplemental Fig. S1). H3K56ac coincides with DNA content, whereas H3K9ac precedes it. Note the different color scales for the epitopes.

To distinguish the contribution of these individual processes to the myc profile, we compared H3 exchange (myc/HA) at each genomic region to both DNA content (the replicated fraction) and to the rate at which this DNA content increases (replication rate) (Fig. 2B,C; Supplemental Fig. S2A,B). Throughout our time course, H3 exchange remained tightly correlated with the replication rate but not with the DNA content (Fig. 2B,C; Supplemental Fig. S2C). Quantitatively, the scaling of H3 exchange at the fork with the replication rate stayed relatively constant throughout the second half of the time course (Fig. 2D). We conclude that in wild-type cells treated with HU, nucleosome incorporation in proximity to the progressing replication fork dominates the nucleosome exchange pattern.

In line with previous studies (Rufiange et al. 2007; Kaplan et al. 2008), we detected a clear correlation between H3K56ac and H3 exchange in nonreplicated cells (Supplemental Fig. S2C) and, accordingly, expected to observe higher exchange in replicated regions in which K56ac accumulates. We noted, however, that the correlation was lost during replication. In particular, H3K56ac was stably maintained after replication concluded, whereas myc was mostly lost (Fig. 1B,C; Supplemental Fig. S1B).

RTT109 deletion reduces nucleosome incorporation at the fork

Our results suggest that H3K56ac does not promote nucleosome exchange, at least during S phase under HU conditions. Because these results are at odds with previous suggestions, we wished to examine the role of H3K56ac in nucleosome exchange more directly. For this, we repeated the experiment in cells deleted of *RTT109* (Supplemental Fig. S3A,B), the only enzyme that deposits this modification (Han et al. 2007). In G_1-arrested cells and at early time points after release, *RTT109* deletion was of little consequence on the exchange of most nucleosomes, with a slightly reduced exchange of the most rapidly exchanging nucleosomes as previously shown (Fig. 3A; Supplemental Fig. S3C,D; Kaplan et al. 2008). The exchange pattern did change, however, once replication progressed: It lost its tight correlation with the replication rate and instead became correlated with the replicated fraction (Fig. 3A,B). This became evident at the later time points, when the replication of early replicating regions approached completion. Of note, the replication pattern, as captured by DNA levels, remained largely invariant to *RTT109* deletion (Supplemental Fig. S3A). Therefore, in *RTT109*-deleted cells, the H3 exchange signal is reduced at the replication fork, while increasing in replicated regions (Fig. 3A,C; Supplemental Fig. S3E).

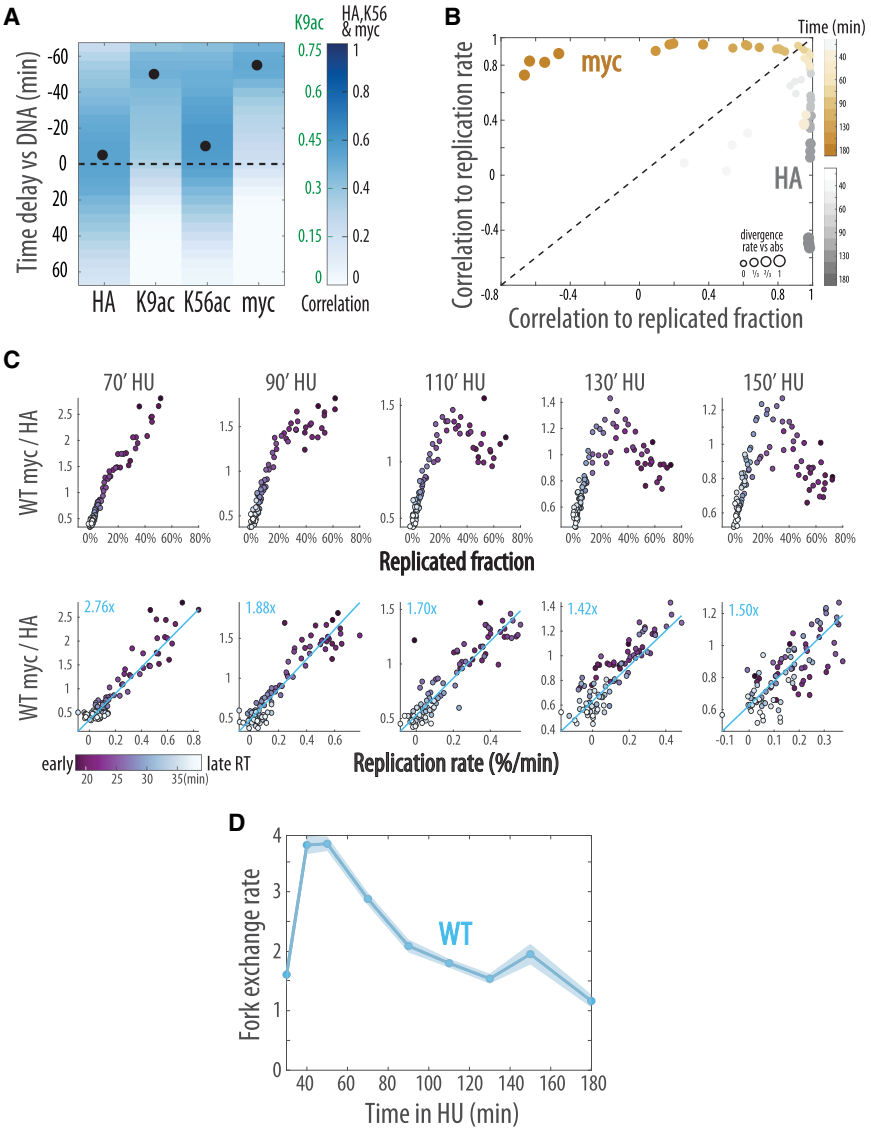

Figure 2. H3 exchange follows replication fork progression. (*A*,*B*) Histone incorporation precedes the replication fork and correlates with the replication rate. (*A*) As in Figure 1E, adding the myc and HA epitope of the exchange sensor marking new and all histones, respectively. Note the different color scales for the epitopes. For additional repeats, see Supplemental Figure S1. n = 4 time courses. (*B*) myc and HA correlation to replication fraction and rate, analyzed as in Figure 1D. (*C*,*D*) Scaling of histone exchange with replicated fraction and replication rate. The genome was clustered based on the annotated RT, and the indicated profile was averaged within each of the 96 clusters (median). (*C*) The average H3 exchange level (myc/HA) as a function of the replicated fraction (*top*) or replication rate (*bottom*). Clusters are colored by their respective RT; time points 70–150 of the time course are shown (for all time points, see Supplemental Fig. S2). The scaling of exchange with the replication rate is summarized in *D*, displaying the slopes of the linear fits in *C* (blue lines) (Supplemental Fig. S2). Shading indicates SE (n = 4).

Because our data are relative, reduced myc levels at the fork could either indicate reduced incorporation at these regions or indicate increased incorporation elsewhere. Refuting the latter possibility, myc levels at rapidly exchanging nucleosomes that have not yet been replicated remained invariant to *RTT109* deletion (Fig. 3D). Wild-type cells therefore show more exchange per replicated nucleosome compared with *RTT109*-deleted cells. We conclude that for a given replicated nucleosome, HU-treated wild-type cells replace multiple nucleosomes at the fork or in its vicinity and that these multiple replacements depend on Rtt109.

Rttl09-dependent H3 N-terminal acetylation is required for fork-associated H3 replacement

Rtt109 thus contributes to nucleosome exchange during slowed DNA replication in two ways: (1) by stabilizing nucleosomes in replicated regions and (2) by increasing nucleosome replacement associated with the progressing fork. As shown above, the two types of Rtt109 acetylation differentially localize to either replicated regions (H3K56ac) or ahead of the progressing fork (H3K9ac). Considering this pattern, we hypothesized that Rtt109 promotes

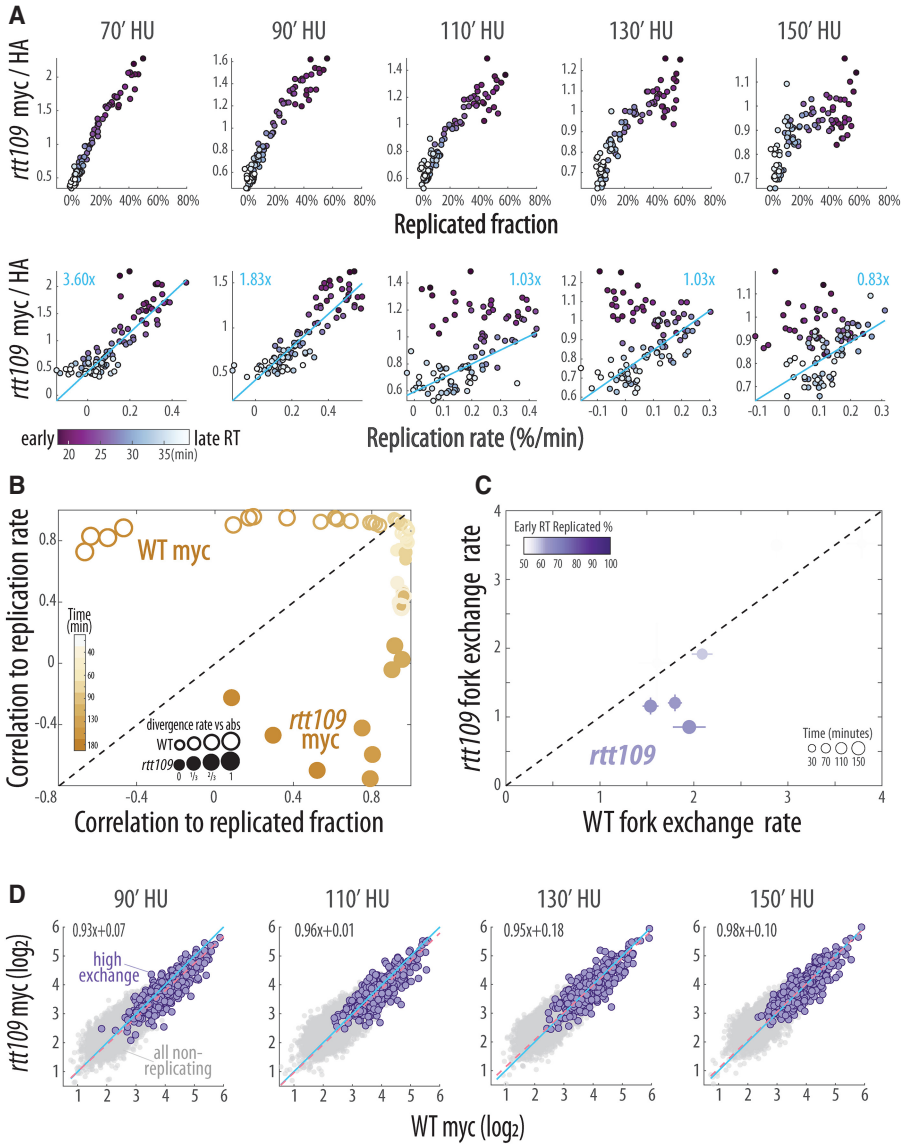

Figure 3. Scaling of H3 exchange with the replication rate depends on Rtt109. (*A*,*B*) Exchange in *RTT109*-deleted cells is dominated by the replicated fraction, rather than the replication rate: (*A*,*B*) As in Figure 2C and 2B, respectively. For all time points, see Supplemental Figure S3. (*C*) Exchange at the replication fork is decreased in *RTT109*-deleted cells. The average fork exchange rate in *RTT109*-deleted cells is plotted against the corresponding rate in wild-type cells. Error bars indicate the SE (n = 3 for *rtt109*, n = 4 for WT). Color intensity indicates the replicated fraction at loci with the earliest RT, and dot size indicates time. (*D*) Replication-independent histone dynamics are invariant to *RTT109* deletion. Mean myc level of nucleosomes that have not yet been replicated at the indicated time points in wild-type versus *RTT109*-deleted cells (n = 4 and 3, respectively). Highlighted are the rapidly exchanging nucleosomes (as determined in G_1 arrest) used for the linear fit (pink dotted line and equation). The one-to-one line is shown in blue.

nucleosome replacement ahead of the fork by acetylating the H3 N terminus while contributing to nucleosome stability in replicated regions through H3K56 acetylation.

To examine this hypothesis, we repeated the experiment in cells deleted of *VPS75* (Fig. 4A; Supplemental Fig. S4A), a chaperone that cooperates with Rtt109 in acetylating the H3 N terminus but is dispensable for H3K56 acetylation. Consistent with this role of *VPS75*, its deletion largely abrogated the replication-associated H3K9ac localization ahead of the fork (Fig. 4B; Supplemental Figs. S4A–C, S5C) while having no effect on H3K56ac (Fig. 4B; Supplemental Fig. S4A,B). Examining the exchange pattern confirmed that *VPS75* deletion specifically reduced fork-associated exchange, resembling the loss of correlation observed in *RTT109*-deleted cells (Fig. 4C; Supplemental Fig. S4D–F). As further predicted, *VPS75* deletion had little effect on the exchange at replicated and nonreplicated regions (Fig. 4A; Supplemental Fig. S4F). Together, we conclude that by acetylating the H3 N terminus, Rtt109 promotes nucleosome replacement ahead of the progressing fork, but H3K9ac does not affect nucleosome exchange in replicated regions.

Discussion

The packaging of eukaryotic genomes within chromatin poses a major obstacle for DNA replication, necessitating the rearrangement of chromatin. In this study, we describe a dual role of Rtt109 in orchestrating nucleosome dynamics during slowed DNA replication, implemented through its distinct activities toward H3K56 and the H3 N terminus. First, by acetylating H3K56, Rtt109 stabilizes nucleosomes at regions already replicated. Second, by acetylating the H3 N terminus, Rtt109 promotes H3 replacement ahead of the replication fork (Fig. 4D).

To increase the resolution at which we follow replication progression, we performed the experiments in HU-treated nucleotide-depleted cells slowing replication. It is possible that this slowing down of replication amplifies the fork-associated exchange we detect. Alternatively, if triggered by fork progression, this exchange might be more pronounced during rapid replication. In addition to slowing replication, nucleotide depletion activates the replication checkpoint, which reduces global histone levels, maintains DNA replication, and stabilizes K56 acetylation (Thaminy et al. 2007; Hauer et al. 2017; Pardo et al. 2017). In particular, the global reduction of histone levels reported to occur in response to HU treatment and DNA damage (Hauer et al. 2017; Hauer and Gasser 2017; Challa et al. 2021) may result from histone loss at the forks. We therefore cannot rule out the contribution of the checkpoint to the increased exchange ahead of the fork. We note, however, that the checkpoint remains intact in *RTT109*-depleted cells, so that Rtt109 is required for this increased exchange independent or downstream from the checkpoint. Moreover, the associated acetylation dynamics also manifest during unperturbed replication (Bar-Ziv et al. 2016), where they contribute to replication regulation (Frenkel et al.

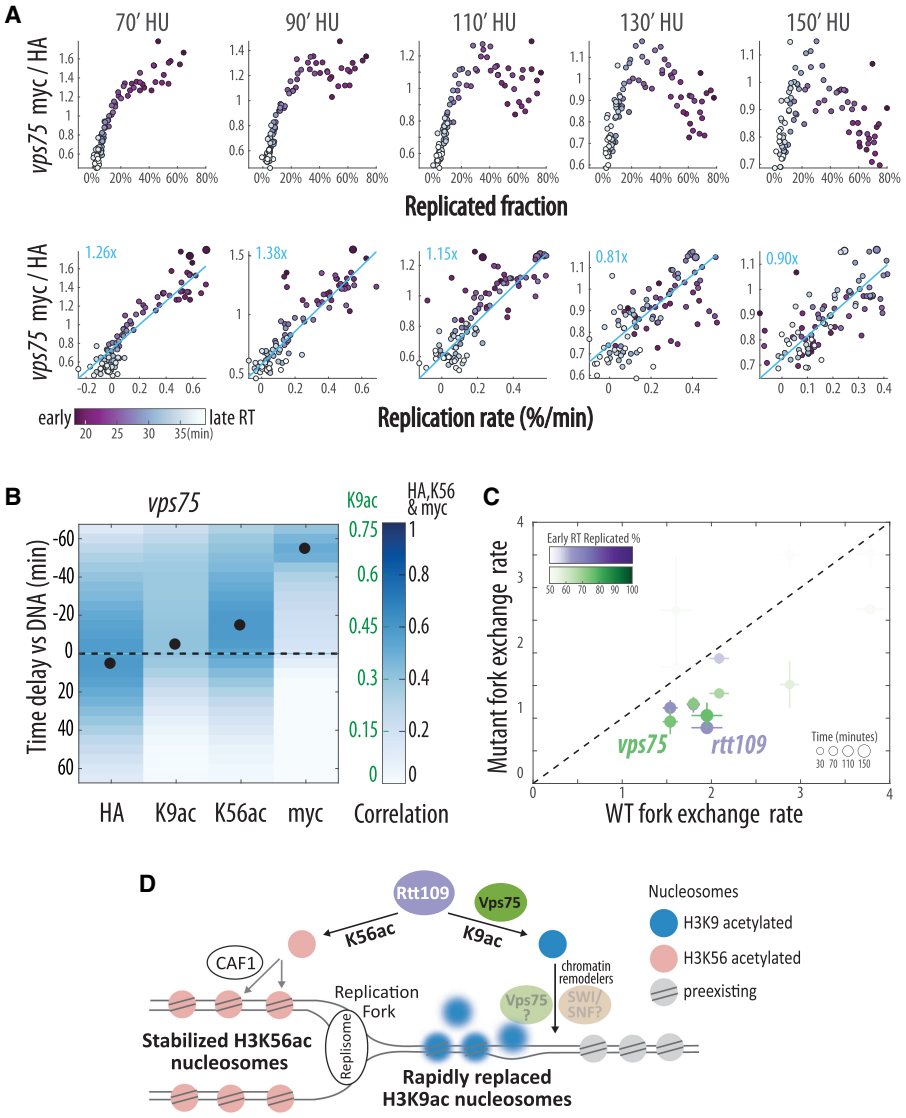

Figure 4. N-terminal H3 acetylation mediates histone exchange ahead of the fork. (*A*–*C*) *VPS75*-deleted cells lose replication-associated K9ac and display reduced H3 exchange ahead of the fork but maintain stable nucleosomes behind it. (*A*,*B*) As in Figure 2C and 2A, respectively, for *VPS75*-deleted cells (n = 2) (see also Supplemental Figure S4). HA data for times 50 and 90 were interpolated (see Methods). Of note is the delayed H3K9 acetylation (*B*; cf. to wild-type cells Fig. 2A; Supplemental Fig. S1A). Note the different color scales for the epitopes. (C) As in Figure 3C with the addition of the *vps75* mutant. (*D*) Rtt109's dual role in regulating histone exchange during DNA replication. A schematic model describing the main findings: Rtt109-dependent acetylation of K56 stabilizes nucleosomes behind the replication fork, whereas acetylation of K9 promotes nucleosome replacement ahead of the fork. See Discussion.

2021). We therefore believe that our findings generalize to unperturbed replication.

The acetylation of H3K56 increases its affinity to CAF1, the histone chaperone that incorporates nucleosomes in the wake of the fork (Li et al. 2008; Han et al. 2013). H3K56ac then accumulates in replicated regions, where it remains throughout S phase. As studies have implicated the H3K56ac modification in promoting the rate of nucleosome exchange (Rufiange et al. 2007; Kaplan et al. 2008; Ferrari and Strubin 2015), we previously suggested that this continuous presence of H3K56ac results from rapid H3 exchange in these regions, thus replenishing H3K56ac from the enriched unbound pool (Voichek et al. 2018). This was supported by a reduced accumulation of position-specific marks through, for example, gene expression, which we previously reported and suggested to contribute to H3K56ac-dependent expression homeostasis (Voichek et al. 2018). Contradicting this hypothesis, our exchange reporter (myc) did disappear from replicated regions displaying high levels of H3K56ac during slow replication. Moreover, deletion of *RTT109* led to a higher, rather than lower, exchange rate in replicated regions. This increased exchange in replicated regions was absent in *vps75*-mutant cells, confirming that H3K56ac was sufficient for stabilizing replicated nucleosomes. Therefore, during slowed S phase, H3K56ac, in addition to promoting CAF1-dependent nucleosome assembly (Topal et al. 2019), acts to stabilize, rather than destabilize, replicated nucleosomes. Whether and how this increased stability contributes to expression homeostasis remain to be studied.

Contrasting H3K56ac, which contributes to expression homeostasis but has no effect on fork velocity, we recently showed that Rtt109-dependent acetylation of the H3 N terminus, which is dispensable for expression homeostasis, slows down replication (Frenkel et al. 2021). Because Rtt109-dependent H3K9ac localizes ahead of the fork, we suggested that this slowdown results from increased nucleosome replacement ahead of the fork (Frenkel et al. 2021). We now provide direct evidence supporting this model: At least in nucleotide-depleted cells, the rapid nucleosome replacement observed in front of the fork is suppressed by deletion of *RTT109* and, more specifically, by deletion of *VPS75*, linking it directly to N-terminal H3 acetylation.

We initially hypothesized that nucleosome replacement ahead of the fork is triggered by the helical stresses that accumulate ahead of the fork and that acetylated H3 is preferentially incorporated in these nucleosome-lacking regions to protect the exposed DNA (Frenkel et al. 2021). However, we could not detect a decrease in nucleosome abundance ahead of the fork in *rtt109* or *vps75* mutants. Neither could we detect expansion of H3K56ac pattern upon *VPS75* deletion, as expected in such a scenario. We therefore find it more likely that Vps75 triggers nucleosome replacement, for example, by first mediating K9ac-dependent chromatin remodeler recruitment to evict histones and then directly promoting histone assembly through Vps75 histone-chaperone activity (Fig. 4D; Selth and Svejstrup 2007). Although such mechanisms could explain the link between K9ac and histone replacement ahead of

the fork, it remains unclear what causes its levels to diminish during fork passage.

Rtt109 is not essential but is required for genome stability (Driscoll et al. 2007; Li et al. 2008). Controlled histone exchange may be the molecular mediator of this function. In replicated regions, increased nucleosome stability is evoked by H3K56 acetylation. At the same time, increased exchange ahead of the fork functions to maintain fork velocity, which could also be important for genomic stability. Indeed, perturbations that either reduced this velocity, like nucleotide depletion (Bester et al. 2011), or increased it, for example, through PARP inhibition (Maya-Mendoza et al. 2018), were found to reduce genome stability. Therefore, Rtt109, through its two distinct functions, regulates nucleosome exchange in apparently opposing ways, compatible with the respective stresses challenging genome stability. Further studies will delineate if these mechanisms are exclusive to DNA replication in HU conditions, as well as evaluate the involvement of the checkpoint.

Methods

Yeast strains

All strains were generated from YGY663 (Yaakov et al. 2021) using standard yeast transformation (Gietz and Schiestl 2007). To prevent competition between tagged and nontagged histone variants, we fused the HA-TEVsite-MYC sensor to Hht2 in YGY663 (in which only Hht1 is tagged), resulting in the H3 double-tagged replicate strains YGY672 and YGY673. We then confirmed almost identical turnover profiles and removal of competition in growing and G_1-arrested yeast cells (see Supplemental Fig. S5A,B). *RTT109* (YGY674 and YGY675) or *VPS75* (YGY721 and YGY722) were deleted using natNT2 or hphNT1 selection markers, respectively (see yeast strains table in Supplemental Material; Janke et al. 2004).

Histone fusions and *BAR1* deletion were introduced using CRISPR-Cas9 as previously described (Yaakov et al. 2021). Sequences including 200 bp upstream of and downstream from the modified histone fusions are provided in Supplemental Material.

Growth conditions

All experiments were performed in YPD media. G_1 synchronization was achieved by incubating 700 mL of exponentially growing (OD_{600} 0.2) *bar1* cells with a final concentration of 5 ng/mL of alpha-factor (GenScript RP01002) for 3 h. The G_1-arrested cells (verified by microscopy) were centrifuged (Sorval SLA-1500, 5 min, 4000*g* at room temperature) in 3 × 250-mL bottles and resuspended in 100 mL prewarmed 30°C YPD supplemented with 50 µg/mL Pronase (Merck 10165921001), at which point the count-up for the time course was initiated. The 2 × 50-mL tubes were centrifuged (1 min, 4000*g* at room temperature) and resuspended in prewarmed 30°C 50 mL YPD supplemented with 50 µg/mL Pronase and 0.2 M HU (Bio Basic HB0528). Cells were pelleted again, resuspended in 550 mL 30°C prewarmed YPD supplemented with 50 µg/mL Pronase and 0.2 M HU, and grown shaking at 30°C for the duration of the time course. Fifty milliliters was taken for each time point: asynchronous (taken aside before alpha-factor was added), alpha-factor arrested (before release), and 15/30/40/50/70/90/110/130/150/180 following release from alpha factor. Each 50 mL sample was crosslinked for 5 min at room temperature in 1% formaldehyde (37% stock Baker, 7040.1000), quenched by adding 0.125 M freshly prepared glycine (Merck G7126) for 5 min at room temperature, washed twice in 50 mL ice-cold water, pelleted, and snap frozen in liquid nitrogen.

DNA library preparation (DNA-seq)

Cells were synchronized and released as above. Growing cells (0.5 mL of exponentially growing cells at OD 0.2 at the time of alpha factor addition) were pipetted directly into 0.6 mL of absolute methanol on dry ice for the duration of the time course. DNA was extracted and sonicated as previously described (Yaakov et al. 2017). Libraries were then prepared (Yaakov et al. 2017), resulting in an average insert size of 180–280 bp.

ChIP-seq

ChIP was performed as previously described (Yaakov et al. 2021). Cell pellets were thawed on ice and washed in 10 mL 1 M sorbitol. After complete liquid removal, pellets were resuspended in 600 µL RIPA buffer (10 mM Tris at pH 8.0, 140 mM NaCl, 1 mM EDTA, 0.1% SDS, 0.1% sodium deoxycholate, 1% Triton X-100, EDTA-free protease inhibitor cocktail) and transferred to chilled LoBind Eppendorf microcentrifuge tubes containing ~500 µL of 0.5-mm zirconium oxide beads (Next Advance ZrOB05). Cells were processed for three cycles in a Bullet blender 24 (Next Advance) at level 8 for 1 min, with 1 min on ice between cycles. Debris and lysate were transferred by piercing a hole in the bottom of the tube, placing a clean chilled tube underneath, and centrifuging at 600*g* for 5 sec at 4°C. The upper tube with the zirconium beads was discarded, and the lysate was hard spun at 17,000*g* for 10 min at 4°C. The supernatant containing cleaved solubilized 8 × myc tags was discarded, and the pellet was thoroughly resuspended in 100 µL NP buffer (10 mM Tris at pH 7.4, 1 M sorbitol, 50 mM NaCl, 5 mM $MgCl_2$, 1 mM $CaCl_2$, and 0.075% NP-40, freshly supplemented with 1 mM β-mercaptoethanol, 500 µM spermidine, and EDTA-free protease inhibitor cocktail), and warmed for 5 min to 37°C in a heat-block . One hundred microliters NP buffer supplemented with 40 units of micrococcal nuclease (Worthington MNase LS004798) was added, and samples were incubated for 20 min at 37°C. The MNase reaction was stopped by adding 200 µL ice-cold stop buffer (220 mM NaCl, 0.2% SDS, 0.2% sodium deoxycholate, 10 mM EDTA, 2%, Triton X-100, EDTA-free protease inhibitor cocktail), vortexing, and placing on ice. Following a 30-min ice incubation, the MNase-treated lysates were centrifuged at 17,000*g* for 10 min at 4°C. MNase digestion resulted in ~90% mononucleosomes and ~10% dinucleosomes, with the latter being filtered out in analysis. This degree of digestion was calibrated per MNase stock and prevents overdigestion by MNase.

The 400 µL supernatant was divided into four separate wells of a 96-well LoBind Eppendorf plate as follows: 110 µL lysate for anti-HA IP (added 10 µL of 12CA5 hybridoma supernatant prepared by the Weizmann Institute in-house Antibody unit), 110 µL lysate for anti-myc (added 10 µL of 9E10 hybridoma supernatant prepared by the Weizmann Institute in-house Antibody unit), 70 µL lysate for anti-H3K9ac (added 5 µg of ab4441), and 70 µL for anti H3K56ac (added 10 µL of rabbit polyclonal anti-H3K56ac kindly provided by Alain Verreault) (Masumoto et al. 2005). Sequencing libraries were prepared as described previously (Yaakov et al. 2021). Full time courses were repeated for all strains: wild-type cells n = 4 for myc and HA, n = 2 for H3K9ac and H3K56ac; *rtt109* cells n = 3 for myc and HA; and *vps75* cells n = 2 for myc, HA, H3K9ac, and H3K56ac.

ChIP-seq and DNA-seq data processing

After demultiplexing, paired-end reads (read1 51 bp, read2 25 bp with NextSeq or 51 bp with NovaSeq) were aligned to the

Saccharomyces cerevisiae genome (R64-1-1) using Bowtie 2 (Langmead and Salzberg 2012) with the following parameters: "-p8 --local --very-sensitive." Aligned reads with sizes 100–200 or zero to 700 bases were then selected and used to calculate the genome coverage using BEDTools (Quinlan and Hall 2010) with the "-pc" option for ChIP-seq or DNA-seq data, respectively. The 100- to 200-bp limit for the ChIP-seq data serves to filter out dinucleosomes and only analyze fragments that came from mononucleosomes. Coverage files were imported into MATLAB and normalized to a total coverage of ~12 Mio across the entire nuclear genome without the ribosomal locus. This normalized coverage was divided into 500-bp bins (or 1 kb for Fig. 1E and similar), and the mean coverage in each bin was calculated. Approximately 3 million aligned genomic reads were obtained per ChIP-seq and DNA-seq sample (either HA, myc, K56ac, or K9ac). For two HA time points with insufficient reads (vps75: repeat 1, 50 and 90 min), the HA profile of each was interpolated as the mean profile of the two adjacent time points, that is, 40 and 70 or 70 and 110, respectively.

ChIP-seq data analysis

DNA replication progression and rate calculation

DNA-seq was performed in two biological repeats for each strain. After confirming a strong correlation between the dynamics of these two time courses, we calculated their mean coverage at each time point and used these combined data for analysis.

ORI-specific analysis

For each time point, the coverage of every 500-bp bin was $\log_2$-normalized to its G_1 coverage using "robustfit." Next, all 358 ORIs in the yeast genome were grouped according to their RT into five ORI clusters. For each ORI cluster, the mean G_1-normalized coverage across all ORIs at different distances (from 0 to 30 kb) was calculated and smoothed using robust local quadratic regression (rloess) over a seven-bin sliding window along the genome. This smoothened average is shown in Figure 1C and analogous. To calculate the correlation with DNA amount or DNA replication speed (Fig. 1D, analogous) at the ORI cluster with the earliest RT for each time point, we first calculated the DNA profile by fitting a five-parameter logistic curve to the smoothened mean G_1-normalized DNA-seq profile. As DNA replication proceeds away from ORIs, the DNA replication rate is proportional to the first derivative of this fit along the distance. For each time point, the Pearson's correlation between the mean G_1-normalized profiles (HA, myc, K56ac, and K9ac) around the earliest replication ORI cluster and the fitted DNA profile and replication rate was calculated and shown in Figure 1D.

Genome-wide analyses

For genome-wide analysis, the 500-bp bins were clustered into 96 replication clusters: first by their RT (48 groups) and then by their replication dynamics in HU (two clusters per group = 96 clusters). For each ChIP sample and DNA-seq sample, we determined the median coverage (not normalized by G_1) and RT in each cluster. As the DNA-seq coverage is relative and does not account for the increase in total DNA during S phase, we next calculated the increase in total DNA, based on the observation that DNA in each cluster only increases concomitantly during S phase (Bar-Ziv et al. 2016; Frenkel et al. 2021). For two consecutive time points, the increase in total DNA was set so that the absolute DNA level of slowest replicating cluster (either the one with the highest RT or the lowest RT, for early and late time point, respectively), with the strongest decrease in relative coverage, stays constant once the change in total DNA is accounted for. Next, the cumulated DNA increase from time 0 up to a given time point was taken as the total DNA level for this time point (raising from one to approximately 1.4 during the time courses). Finally, for each time point, the absolute DNA level in each cluster results from multiplying a cluster's relative DNA level with the time point's total DNA, and the replicated fraction (Fig. 2C) by subtracting one. The replication rate in cluster i at time point t, $r(i,t)$, is calculated as

$$r(i,t) = 0.5 \times [\mathrm{DNA_{abs}}(i,t) - \mathrm{DNA_{abs}}(i,t-1)]/[T_t - T_{t-1}] + 0.5 \times [\mathrm{DNA_{abs}}(i,t+1) - \mathrm{DNA_{abs}}(i,t)]/[T_{t+1} - T_t],$$

where $\mathrm{DNA_{abs}}$ is the absolute DNA level in cluster i at time point t, and T_t is the time since HU release at time point t.

For Figure 2C, the ratio median myc over median HA level (not absolute) of each cluster at every time point is compared against its current replication rate or replicated fraction (Pearson's correlation of all time courses is summarized in Supplemental Fig. S2B). The fork-dependent turnover (Fig. 2C,D) is calculated as the slope of the robust linear fit (robustfit) between the myc–HA ratio and the replication rate. The fork-dependent turnover across all time points is summarized in Figure 2D and similar.

Time delay analysis

To calculate the time delay (Fig. 1E) between the DNA-seq dynamics and those of the different epitopes (HA, myc, K9ac, and K56ac), the genome was divided into 2-kb bins, and the mean coverage in each bin was calculated. Notably, smaller bin sizes like 500 bp give very similar results but with lower correlations (see Supplemental Fig. S5C). In particular, for K9ac the 2-kb bin reduces the impact of the replication-independent component. For every sample in a time course, the epitope level of every bin was $\log_2$-normalized against the corresponding level in alpha factor arrest (G_1) using robust fit, and the resulting level was smoothened along the genome using local robust linear regression with a six-bin window.

Afterward, the G_1-normalized dynamics across the time course were fitted with a smoothing spline and the fit used to interpolate the change in 5-min intervals. Next, we correlated the change across all bins in DNA level at each interpolated time point with the change in the other epitopes at every other time point (n^2 correlations for n interpolated time points). The correlation for each delay and epitope, tau, is calculated as the mean correlation, Cr, between each time point pair after the onset of DNA replication ($t = 30$ min) separated by a certain delay:

$$Cr\mathrm{K56ac}(\tau = -15\,\mathrm{min}) = \mathrm{mean}(cr(\Delta\mathrm{DNA}_{45}, \Delta\mathrm{K56ac}_{30}), cr(\Delta\mathrm{DNA}_{50}, \Delta\mathrm{K56ac}_{35}), \ldots, cr(\Delta\mathrm{HA}_{100}, \Delta\mathrm{K56ac}_{85})).$$

$cr(x,x)$ is Pearson's correlation between two samples, and ΔXX_t is the interpolated change of epitope XX at time point t. To have a similar number of comparisons with longer delays, we only compared DNA time points up to 100 min after HU exposure.

Nucleosome-specific processing

Nucleosomes were analyzed as described previously (Yaakov et al. 2021). In brief, genome-wide coverage was normalized to a total coverage of 10^8, and the mean normalized coverage of 100 bp around each nucleosome position (±50 bp) was calculated.

$\mathrm{Log_2}$ turnover (myc/HA) and epitope enrichment (K56/HA), Enr$X$, for each nucleosome (Supplemental Fig. S2C) were calculated as follows: $\mathrm{Enr}X = \log_2(X(i,t)+1) - \log_2(\mathrm{HA}(i,t)+1)$, where $X(i,t)$ is the level of epitope X on nucleosome i at time point t.

Late replicating and highly turning over nucleosomes (Fig. 3D) were selected based on the RT cluster with <10% replication at the last time point across all time course (mean) and a mean turnover ($\log_2$(myc/HA)) greater than 1.5 in G_1-arrested cells, respectively.

For HA/H3 level by RT analysis (Supplemental Fig. S5), each nucleosome was assigned an RT based on its position, and the mean epitope level across all nucleosomes with a particular RT (±1 min) was calculated and shown.

Data access

All raw and processed sequencing data generated in this study have been submitted to the NCBI Gene Expression Omnibus (GEO; https://www.ncbi.nlm.nih.gov/geo/) under accession numbers GSE193044 and GSE157402. All MATLAB scripts to analyze the data and generate the figures can be found in the Supplemental Code and on GitHub (https://github.com/barkailab/Jonas2022).

Competing interest statement

The authors declare no competing interests.

Acknowledgments

We thank Y. Voichek and N. Frenkel for comments on the manuscript. We thank our laboratory members for discussions throughout. We thank Alain Verreault for the H3K56ac antibody. This work was funded by the Israel Science Foundation FIRST Program (grant no. 966/19), Horizon Europe (European Research Council), and the Minerva Foundation.

Author contributions: F.J. performed all analyses. G.Y. performed all experiments. All authors designed the experiments, discussed the results, and wrote the paper.

References

Ahmad K, Henikoff S. 2002. The histone variant H3.3 marks active chromatin by replication-independent nucleosome assembly. *Mol Cell* **9:** 1191–1200. doi:10.1016/S1097-2765(02)00542-7

Andrews AJ, Luger K. 2011. Nucleosome structure(s) and stability: variations on a theme. *Annu Rev Biophys* **40:** 99–117. doi:10.1146/annurev-biophys-042910-155329

Bannister AJ, Kouzarides T. 2011. Regulation of chromatin by histone modifications. *Cell Res* **21:** 381–395. doi:10.1038/cr.2011.22

Bar-Ziv R, Voichek Y, Barkai N. 2016. Chromatin dynamics during DNA replication. *Genome Res* **26:** 1245–1256. doi:10.1101/gr.201244.115

Bar-Ziv R, Brodsky S, Chapal M, Barkai N. 2020. Transcription factor binding to replicated DNA. *Cell Rep* **30:** 3989–3995.e4. doi:10.1016/j.celrep.2020.02.114

Bauer WR, Hayes JJ, White JH, Wolffe AP. 1994. Nucleosome structural changes due to acetylation. *J Mol Biol* **236:** 685–690. doi:10.1006/jmbi.1994.1180

Bechhoefer J, Rhind N. 2012. Replication timing and its emergence from stochastic processes. *Trends Genet* **28:** 374–381. doi:10.1016/j.tig.2012.03.011

Berndsen CE, Tsubota T, Lindner SE, Lee S, Holton JM, Kaufman PD, Keck JL, Denu JM. 2008. Molecular functions of the histone acetyltransferase chaperone complex Rtt109–Vps75. *Nat Struct Mol Biol* **15:** 948–956. doi:10.1038/nsmb.1459

Bester AC, Roniger M, Oren YS, Im MM, Sarni D, Chaoat M, Bensimon A, Zamir G, Shewach DS, Kerem B. 2011. Nucleotide deficiency promotes genomic instability in early stages of cancer development. *Cell* **145:** 435–446. doi:10.1016/j.cell.2011.03.044

Bondarenko VA, Steele LM, Újvári A, Gaykalova DA, Kulaeva OI, Polikanov YS, Luse DS, Studitsky VM. 2006. Nucleosomes can form a polar barrier to transcript elongation by RNA polymerase II. *Mol Cell* **24:** 469–479. doi:10.1016/j.molcel.2006.09.009

Celic I, Masumoto H, Griffith WP, Meluh P, Cotter RJ, Boeke JD, Verreault A. 2006. The sirtuins Hst3 and Hst4p preserve genome integrity by controlling histone H3 lysine 56 deacetylation. *Curr Biol* **16:** 1280–1289. doi:10.1016/j.cub.2006.06.023

Challa K, Schmid CD, Kitagawa S, Cheblal A, Iesmantavicius V, Seeber A, Amitai A, Seebacher J, Hauer MH, Shimada K, et al. 2021. Damage-induced chromatome dynamics link ubiquitin ligase and proteasome recruitment to histone loss and efficient DNA repair. *Mol Cell* **81:** 811–829.e6. doi:10.1016/j.molcel.2020.12.021

Chatterjee N, Sinha D, Lemma-Dechassa M, Tan S, Shogren-Knaak MA, Bartholomew B. 2011. Histone H3 tail acetylation modulates ATP-dependent remodeling through multiple mechanisms. *Nucleic Acids Res* **39:** 8378–8391. doi:10.1093/nar/gkr535

Clapier CR, Iwasa J, Cairns BR, Peterson CL. 2017. Mechanisms of action and regulation of ATP-dependent chromatin-remodelling complexes. *Nat Rev Mol Cell Biol* **18:** 407–422. doi:10.1038/nrm.2017.26

Corless S, Gilbert N. 2016. Effects of DNA supercoiling on chromatin architecture. *Biophys Rev* **8:** 245–258. doi:10.1007/s12551-016-0210-1

Das C, Tyler JK. 2013. Histone exchange and histone modifications during transcription and aging. *Biochim Biophys Acta* **1819:** 332–342. doi:10.1016/j.bbagrm.2011.08.001

Dilworth SM, Dingwall C. 1988. Chromatin assembly *in vitro* and *in vivo*. *Bioessays* **9:** 44–49. doi:10.1002/bies.950090203

Dion MF, Kaplan T, Kim M, Buratowski S, Friedman N, Rando OJ. 2007. Dynamics of replication-independent histone turnover in budding yeast. *Science* **315:** 1405–1408. doi:10.1126/science.1134053

Driscoll R, Hudson A, Jackson SP. 2007. Yeast Rtt109 promotes genome stability by acetylating histone H3 on lysine 56. *Science* **315:** 649–652. doi:10.1126/science.1135862

Ferrari P, Strubin M. 2015. Uncoupling histone turnover from transcription-associated histone H3 modifications. *Nucleic Acids Res* **43:** 3972–3985. doi:10.1093/nar/gkv282

Fillingham J, Recht J, Silva AC, Suter B, Emili A, Stagljar I, Krogan NJ, Allis CD, Keogh M-C, Greenblatt JF. 2008. Chaperone control of the activity and specificity of the histone H3 acetyltransferase Rtt109. *Mol Cell Biol* **28:** 4342–4353. doi:10.1128/MCB.00182-08

Fleming AB, Kao C-F, Hillyer C, Pikaart M, Osley MA. 2008. H2b ubiquitylation plays a role in nucleosome dynamics during transcription elongation. *Mol Cell* **31:** 57–66. doi:10.1016/j.molcel.2008.04.025

Frenkel N, Jonas F, Carmi M, Yaakov G, Barkai N. 2021. Rtt109 slows replication speed by histone N-terminal acetylation. *Genome Res* **31:** 426–435. doi:10.1101/gr.266510.120

Gietz RD, Schiestl RH. 2007. High-efficiency yeast transformation using the LiAc/SS carrier DNA/PEG method. *Nat Protoc* **2:** 31–34. doi:10.1038/nprot.2007.13

Groth A, Rocha W, Verreault A, Almouzni G. 2007. Chromatin challenges during DNA replication and repair. *Cell* **128:** 721–733. doi:10.1016/j.cell.2007.01.030

Ha M, Kraushaar DC, Zhao K. 2014. Genome-wide analysis of H3.3 dissociation reveals high nucleosome turnover at distal regulatory regions of embryonic stem cells. *Epigenetics Chromatin* **7:** 38. doi:10.1186/1756-8935-7-38

Hammond CM, Strømme CB, Huang H, Patel DJ, Groth A. 2017. Histone chaperone networks shaping chromatin function. *Nat Rev Mol Cell Biol* **18:** 141–158. doi:10.1038/nrm.2016.159

Hamperl S, Cimprich KA. 2016. Conflict resolution in the genome: how transcription and replication make it work. *Cell* **167:** 1455–1467. doi:10.1016/j.cell.2016.09.053

Han J, Zhou H, Horazdovsky B, Zhang K, Xu R-M, Zhang Z. 2007. Rtt109 acetylates histone H3 lysine 56 and functions in DNA replication. *Science* **315:** 653–655. doi:10.1126/science.1133234

Han J, Zhang H, Zhang H, Wang Z, Zhou H, Zhang Z. 2013. A Cul4 E3 ubiquitin ligase regulates histone hand-off during nucleosome assembly. *Cell* **155:** 817–829. doi:10.1016/j.cell.2013.10.014

Hauer MH, Gasser SM. 2017. Chromatin and nucleosome dynamics in DNA damage and repair. *Genes Dev* **31:** 2204–2221. doi:10.1101/gad.307702.117

Hauer MH, Seeber A, Singh V, Thierry R, Sack R, Amitai A, Kryzhanovska M, Eglinger J, Holcman D, Owen-Hughes T, et al. 2017. Histone degradation in response to DNA damage enhances chromatin dynamics and recombination rates. *Nat Struct Mol Biol* **24:** 99–107. doi:10.1038/nsmb.3347

Hong L, Schroth GP, Matthews HR, Yau P, Bradbury EM. 1993. Studies of the DNA binding properties of histone H4 amino terminus: Thermal denaturation studies reveal that acetylation markedly reduces the binding constant of the H4 "tail" to DNA. *J Biol Chem* **268:** 305–314. doi:10.1016/S0021-9258(18)54150-8

Hsieh F-K, Kulaeva OI, Patel SS, Dyer PN, Luger K, Reinberg D, Studitsky VM. 2013. Histone chaperone FACT action during transcription through chromatin by RNA polymerase II. *Proc Natl Acad Sci* **110:** 7654–7659. doi:10.1073/pnas.1222198110

Huang C, Zhang Z, Xu M, Li Y, Li Z, Ma Y, Cai T, Zhu B. 2013. H3.3-H4 tetramer splitting events feature cell-type specific enhancers. *PLoS Genet* **9:** e1003558. doi:10.1371/journal.pgen.1003558

Ito T, Bulger M, Kobayashi R, Kadonaga JT. 1996. *Drosophila* NAP-1 is a core histone chaperone that functions in ATP-facilitated assembly of regularly spaced nucleosomal arrays. *Mol Cell Biol* **16:** 3112–3124. doi:10.1128/MCB.16.6.3112

Janke C, Magiera MM, Rathfelder N, Taxis C, Reber S, Maekawa H, Moreno-Borchart A, Doenges G, Schwob E, Schiebel E, et al. 2004. A versatile toolbox for PCR-based tagging of yeast genes: new fluorescent proteins, more markers and promoter substitution cassettes. *Yeast* **21:** 947–962. doi:10.1002/yea.1142

Kaplan T, Liu CL, Erkmann JA, Holik J, Grunstein M, Kaufman PD, Friedman N, Rando OJ. 2008. Cell cycle- and chaperone-mediated regulation of H3K56ac incorporation in yeast. *PLoS Genet* **4:** e1000270. doi:10.1371/journal.pgen.1000270

Keppler A, Pick H, Arrivoli C, Vogel H, Johnsson K. 2004. Labeling of fusion proteins with synthetic fluorophores in live cells. *Proc Natl Acad Sci* **101:** 9955–9959. doi:10.1073/pnas.0401923101

Kraushaar DC, Jin W, Maunakea A, Abraham B, Ha M, Zhao K. 2013. Genome-wide incorporation dynamics reveal distinct categories of turnover for the histone variant H3.3. *Genome Biol* **14:** R121. doi:10.1186/gb-2013-14-10-r121

Kristjuhan A, Svejstrup JQ. 2004. Evidence for distinct mechanisms facilitating transcript elongation through chromatin *in vivo*. *EMBO J* **23:** 4243–4252. doi:10.1038/sj.emboj.7600433

Lai WKM, Pugh BF. 2017. Understanding nucleosome dynamics and their links to gene expression and DNA replication. *Nat Rev Mol Cell Biol* **18:** 548–562. doi:10.1038/nrm.2017.47

Langmead B, Salzberg SL. 2012. Fast gapped-read alignment with Bowtie 2. *Nat Methods* **9:** 357–359. doi:10.1038/nmeth.1923

Laskey R, Honda B, Mills A, Finch J. 1978. Nucleosomes are assembled by an acidic protein which binds histones and transfers them to DNA. *Nature* **275:** 416–420. doi:10.1038/275416a0

Lee J, Lee T-H. 2019. How protein binding sensitizes the nucleosome to histone H3K56 acetylation. *ACS Chem Biol* **14:** 506–515. doi:10.1021/acschembio.9b00018

Lee DY, Hayes JJ, Pruss D, Wolffe AP. 1993. A positive role for histone acetylation in transcription factor access to nucleosomal DNA. *Cell* **72:** 73–84. doi:10.1016/0092-8674(93)90051-Q

Li Q, Zhou H, Wurtele H, Davies B, Horazdovsky B, Verreault A, Zhang Z. 2008. Acetylation of histone H3 lysine 56 regulates replication-coupled nucleosome assembly. *Cell* **134:** 244–255. doi:10.1016/j.cell.2008.06.018

Luger K, Mäder AW, Richmond RK, Sargent DF, Richmond TJ. 1997. Crystal structure of the nucleosome core particle at 2.8 Å resolution. *Nature* **389:** 251–260. doi:10.1038/38444

Maas NL, Miller KM, DeFazio LG, Toczyski DP. 2006. Cell cycle and checkpoint regulation of histone H3 K56 acetylation by Hst3 and Hst4. *Mol Cell* **23:** 109–119. doi:10.1016/j.molcel.2006.06.006

Masumoto H, Hawke D, Kobayashi R, Verreault A. 2005. A role for cell-cycle-regulated histone H3 lysine 56 acetylation in the DNA damage response. *Nature* **436:** 294–298. doi:10.1038/nature03714

Mattiroli F, D'Arcy S, Luger K. 2015. The right place at the right time: chaperoning core histone variants. *EMBO Rep* **16:** 1454–1466. doi:10.15252/embr.201540840

Maya-Mendoza A, Moudry P, Merchut-Maya JM, Lee M, Strauss R, Bartek J. 2018. High speed of fork progression induces DNA replication stress and genomic instability. *Nature* **559:** 279–284. doi:10.1038/s41586-018-0261-5

Owen-Hughes T, Gkikopoulos T. 2012. Making sense of transcribing chromatin. *Curr Opin Cell Biol* **24:** 296–304. doi:10.1016/j.ceb.2012.02.003

Pardo B, Crabbé L, Pasero P. 2017. Signaling pathways of replication stress in yeast. *FEMS Yeast Res* **17:** fow101. doi:10.1093/femsyr/fow101

Quinlan AR, Hall IM. 2010. BEDTools: a flexible suite of utilities for comparing genomic features. *Bioinformatics* **26:** 841–842. doi:10.1093/bioinformatics/btq033

Radman-Livaja M, Verzijlbergen KF, Weiner A, van Welsem T, Friedman N, Rando OJ, van Leeuwen F. 2011. Patterns and mechanisms of ancestral histone protein inheritance in budding yeast. *PLoS Biol* **9:** e1001075. doi:10.1371/journal.pbio.1001075

Rufiange A, Jacques PE, Bhat W, Robert F, Nourani A. 2007. Genome-wide replication-independent histone H3 exchange occurs predominantly at promoters and implicates H3 K56 acetylation and Asf1. *Mol Cell* **27:** 393–405. doi:10.1016/j.molcel.2007.07.011

Sadeghi L, Prasad P, Ekwall K, Cohen A, Svensson JP. 2015. The Paf1 complex factors Leo1 and Paf1 promote local histone turnover to modulate chromatin states in fission yeast. *EMBO Rep* **16:** 1673–1687. doi:10.15252/embr.201541214

Schermer UJ, Korber P, Hörz W. 2005. Histones are incorporated in *trans* during reassembly of the yeast *PHO5* promoter. *Mol Cell* **19:** 279–285. doi:10.1016/j.molcel.2005.05.028

Schwabish MA, Struhl K. 2004. Evidence for eviction and rapid deposition of histones upon transcriptional elongation by RNA polymerase II. *Mol Cell Biol* **24:** 10111–10117. doi:10.1128/MCB.24.23.10111-10117.2004

Selth L, Svejstrup JQ. 2007. Vps75, a new yeast member of the NAP histone chaperone family. *J Biol Chem* **282:** 12358–12362. doi:10.1074/jbc.C700012200

Siow CC, Nieduszynska SR, Müller CA, Nieduszynski CA. 2012. OriDB, the DNA replication origin database updated and extended. *Nucleic Acids Res* **40:** D682–D686. doi:10.1093/nar/gkr1091

Siwek W, Gómez-Rodríguez M, Sobral D, Corrêa IR, Jansen LET. 2018. time-ChIP: a method to determine long-term locus-specific nucleosome inheritance. In *Histone variants: methods and protocols* (ed. Orsi GA, Almouzni G), pp. 131–158. Springer, New York.

Smolle M, Venkatesh S, Gogol MM, Li H, Zhang Y, Florens L, Washburn MP, Workman JL. 2012. Chromatin remodelers Isw1 and Chd1 maintain chromatin structure during transcription by preventing histone exchange. *Nat Struct Mol Biol* **19:** 884–892. doi:10.1038/nsmb.2312

Thaminy S, Newcomb B, Kim J, Gatbonton T, Foss E, Simon J, Bedalov A. 2007. Hst3 is regulated by Mec1-dependent proteolysis and controls the S phase checkpoint and sister chromatid cohesion by deacetylating histone H3 at lysine 56. *J Biol Chem* **282:** 37805–37814. doi:10.1074/jbc.M706384200

Topal S, Vasseur P, Radman-Livaja M, Peterson CL. 2019. Distinct transcriptional roles for histone H3-K56 acetylation during the cell cycle in yeast. *Nat Commun* **10:** 4372. doi:10.1038/s41467-019-12400-5

Tsubota T, Berndsen CE, Erkmann JA, Smith CL, Yang L, Freitas MA, Denu JM, Kaufman PD. 2007. Histone H3-K56 acetylation is catalyzed by histone chaperone-dependent complexes. *Mol Cell* **25:** 703–712. doi:10.1016/j.molcel.2007.02.006

Venkatesh S, Smolle M, Li H, Gogol MM, Saint M, Kumar S, Natarajan K, Workman JL. 2012. Set2 methylation of histone H3 lysine 36 suppresses histone exchange on transcribed genes. *Nature* **489:** 452–455. doi:10.1038/nature11326

Verreault A, Kaufman PD, Kobayashi R, Stillman B. 1996. Nucleosome assembly by a complex of CAF-1 and acetylated histones H3/H4. *Cell* **87:** 95–104. doi:10.1016/S0092-8674(00)81326-4

Verzijlbergen KF, Menendez-Benito V, van Welsem T, van Deventer SJ, Lindstrom DL, Ovaa H, Neefjes J, Gottschling DE, van Leeuwen F. 2010. Recombination-induced tag exchange to track old and new proteins. *Proc Natl Acad Sci* **107:** 64–68. doi:10.1073/pnas.0911164107

Verzijlbergen KF, van Welsem T, Sie D, Lenstra TL, Turner DJ, Holstege FC, Kerkhoven RM, van Leeuwen F. 2011. A barcode screen for epigenetic regulators reveals a role for the NuB4/HAT-B histone acetyltransferase complex in histone turnover. *PLoS Genet* **7:** e1002284. doi:10.1371/journal.pgen.1002284

Voichek Y, Bar-Ziv R, Barkai N. 2016a. A role for Rtt109 in buffering gene-dosage imbalance during DNA replication. *Nucleus* **7:** 375–381. doi:10.1080/19491034.2016.1216743

Voichek Y, Bar-Ziv R, Barkai N. 2016b. Expression homeostasis during DNA replication. *Science* **351:** 1087–1090. doi:10.1126/science.aad1162

Voichek Y, Mittelman K, Gordon Y, Bar-Ziv R, Lifshitz Smit D, Shenhav R, Barkai N. 2018. Epigenetic control of expression homeostasis during replication is stabilized by the replication checkpoint. *Mol Cell* **70:** 1121–1133.e9. doi:10.1016/j.molcel.2018.05.015

Yaakov G, Lerner D, Bentele K, Steinberger J, Barkai N. 2017. Coupling phenotypic persistence to DNA damage increases genetic diversity in severe stress. *Nat Ecol Evol* **1:** 16. doi:10.1038/s41559-016-0016

Yaakov G, Jonas F, Barkai N. 2021. Measurement of histone replacement dynamics with genetically encoded exchange timers in yeast. *Nat Biotechnol* **39:** 1467. doi:10.1038/s41587-021-01103-2

Yabuki N, Terashima H, Kitada K. 2002. Mapping of early firing origins on a replication profile of budding yeast. *Genes Cells* **7:** 781–789. doi:10.1046/j.1365-2443.2002.00559.x

Yildirim O, Hung JH, Cedeno RJ, Weng Z, Lengner CJ, Rando OJ. 2014. A system for genome-wide histone variant dynamics in ES cells reveals dynamic MacroH2A2 replacement at promoters. *PLoS Genet* **10:** e1004515. doi:10.1371/journal.pgen.1004515

Zhang Q, Chakravarty S, Ghersi D, Zeng L, Plotnikov AN, Sanchez R, Zhou MM. 2010. Biochemical profiling of histone binding selectivity of the yeast bromodomain family. *PLoS One* **5:** e8903. doi:10.1371/journal.pone.0008903

Received February 9, 2022; accepted in revised form May 5, 2022.